High resolution measurement of the $^{16}O(\gamma,pn)^{14}N_{0,1,2,\ldots}$ reaction

K. R. Garrow,* F. Adimi, N. R. Kolb, J. Lu, R. E. Pywell, D. M. Skopik,* and J. M. Vogt
Saskatchewan Accelerator Laboratory, University of Saskatchewan, Saskatoon, Saskatchewan, Canada S7N 5C6

J. W. Jury
Department of Physics, Trent University, Peterborough, Ontario, Canada K9J 7B8

A. Kuzin and M. N. Thompson
School of Physics, University of Melbourne, Parkville, 3052 Australia

J. Ryckebusch
Department of Subatomic and Radiation Physics, University of Gent, Proeftuinstraat 86, B-9000 Gent, Belgium
(Received 23 May 2001; published 5 November 2001)

The exclusive $^{16}O(\gamma,pn)^{14}N_{0,1,2,\ldots}$ reaction was measured for the photon energy range $E_\gamma = 98.5$ to 141.0 MeV with an excitation energy resolution of 2.8 MeV. Protons were detected at 76° and 82° and coincident neutrons were detected at the opening angle for quasifree deuteron photodisintegration. Only the $T=0$, 1^+, 3.95 MeV state in the residual ^{14}N nucleus was significantly populated. This corresponds to a preferred $L=0$ angular momentum transfer to the recoil nucleus as is expected for quasifree kinematics. The absence of significant population to other discrete states is evidence that absorption on correlated proton-neutron pairs with an angular momentum transfer of $L \geqslant 2$ is largely suppressed for the low recoil momentum range of the current measurement. As a consequence of this fact, and the absence of unnatural parity states, only absorption on proton-neutron pairs in relative motion $l=0,2$ is expected for all possible shell model couplings. No significant population of the $T=1$ state at 2.31 MeV is consistent with previous measurements, demonstrating that absorption on proton-neutron pairs in an isospin triplet is suppressed. The results of the measurement to discrete states in the residual ^{14}N nucleus are compared to microscopic calculations which include contributions above that of the mean field due to the short range and tensor parts of the nuclear potential. Clear separation in the contribution of $(1p)^{-2}$ and $(1p)^{-1}(1s)^{-1}$ proton-neutron pairs is seen to occur at an excitation energy of 20 ± 2 MeV. Significant population of the $(1p)^{-1}(1s)^{-1}$ continuum above 20 MeV indicates that absorption on $L=1$ nucleon pairs is also important near quasifree kinematics.

DOI: 10.1103/PhysRevC.64.064602 PACS number(s): 25.20.Lj, 27.20.+n

I. INTRODUCTION

Historically, it was the very pronounced forward peaking observed in the proton angular distribution which provided the first indication, based on a kinematical interpretation, that the photon ($E_\gamma \geqslant \sim 100$ MeV) is absorbed by a small subunit within the nucleus rather than by the nucleus as a whole. This observation from early bremsstralung experiments, in conjunction with the known fact that the photodisintegration of the deuteron is dominated by electric dipole absorption, inspired Levinger [1] to propose the phenomenological quasideuteron (QD) mechanism for the photodisintegration of complex nuclei. Verification of this model was obtained by double arm experiments [2,3] in which protons and neutrons were detected in coincidence. The results bore a striking resemblance to the photodisintegration of deuterium except that the angular correlation of the pn pair was broadened compared to the exact angular correlation of deuterium. This observation was assumed to result from the Fermi motion of the pn pair and corresponds to the back-to-back emission of the correlated pn pair in the center-of-mass frame defined by the photon and the ejected pair.

A more detailed calculation for the two nucleon photoabsorption process was developed by Gottfried [4]. Based on a spectator model for the $A-2$ recoil nucleus, it was shown that the $(\gamma,2N)$ cross section could be written in a factorized form. In this model, the cross section is proportional to the available phase space and two other terms. A form factor $F(P)$ defined as the probability of finding a pn pair with zero separation and moving with a momentum P within the nucleus, and a term S_{fi} defined as the product of two correlation functions, one which results from Pauli correlations while the other is sensitive to the more interesting short-range correlations (SRC). Gottfried goes on to show that for completely closed shell nuclei the (γ,pn) interaction can be expressed in terms of the elementary deuterium cross section evaluated off the energy shell. This result is similar to Levinger's original model.

Identifying particular shell couplings in the missing (γ,pn) energy spectra can provide a test of the impulse approximation or spectator model for the recoil $A-2$ nucleus. In such a model the initial momentum of the pn pair is equal and opposite to the recoil momentum of the residual nucleus. McGeorge *et al.* [5] compare their $^{12}C(\gamma,pn)^{10}B$ recoil momentum data with momentum distributions derived from distinct two nucleon wave functions resulting from the different possible shell couplings, and determined that photon absorp-

*Present address: TJNAF, Newport News, VA 23606.

tion on two nucleons was the dominant interaction mode for the energy range $E_\gamma = 80$–157 MeV. The authors find that the agreement of their two nucleon calculation, with considerations made for final-state interactions (FSI's), accounts for all the measured $^{12}C(\gamma,pn)^{10}B$ yield without the need for introducing other absorption mechanisms. An earlier measurement by MacGregor *et al.* [6] of the $^{16}O(\gamma,pn)^{14}N$ reaction for the photon energy range $E_\gamma = 80$–131 MeV and covering a significant part of phase space, provided the first indication that more than one discrete state was excited in the ^{14}N nucleus. Their results indicated a significant yield in the excitation energy spectrum centered at about 4 MeV. Although their energy resolution was not sufficient to resolve the residual states the width of the peak was larger than that expected for their energy resolution, indicating that more than one discrete state was excited in the ^{14}N nucleus.

The purpose of the present measurement was to learn more about the reaction mechanism on a microscopic level. Determining the relevant quantum numbers involved in the photoabsorption process has been a long outstanding problem. For instance, the possibility of the two nucleon system being in an isospin triplet during the absorption process cannot be ruled out. Experimental evidence for real photon absorption on $T=1$ pairs has been reported [7]. Observed states which are more strongly populated in the (γ,p) channel than that for the $(e,e'p)$ reaction were noted to have a $1p$-$2h$ character. This was inferred to suggest a two nucleon absorption mechanism for the incoming photon. The moderately high resolution data indicated that transitions to $1p$-$2h$ states in the $A-1$ nucleus were populated with significant strength. Such $1p$-$2h$ configurations are known to have a high percentage of $T=1$, $2h$ states in the residual $A-1$ nucleus. This was interpreted as evidence for absorption on $T=1$ proton-neutron pairs for intermediate photon energies. A further indication for the absorption on $T=1$ proton-neutron pairs was seen by significant population to the isospin forbidden state in the $^{12}C(e,e'd)^{10}B_{T=1}$ measurement [8]. The mechanism was postulated to be an integration of a pn pair in a ^1S state via spin and isospin flip transitions resulting in the emission of a real deuteron. This mechanism was found to be consistent with the experimentally determined purely transverse character of the transition and the four momentum dependence of the cross section.

When performing a measurement of correlated particles with limited solid angle coverage, as in the present case, it is imperative to have an understanding of the form factor, $F(P)$, describing the center-of-mass motion of the pn pair with respect to the $A-2$ spectator nucleus. The shapes of the angular correlation and energy sharing distributions between the emitted nucleon pair are driven by the form factor $F(P)$, which depends on the angular momentum quantum number, L, which characterizes the center-of-mass motion of the correlated pair with respect to the $A-2$ nucleus. For $L=0$ transfer, the form factor peaks at zero recoil momentum for the spectator nucleus, resulting in the angular correlation of the emitted nucleons to be peaked at the quasifree angle and the energy sharing distribution to be peaked at the quasifree energy. For angular momentum transfer values, $L>0$, the form factor vanishes at zero recoil momentum and peaks at positive and negative values of the recoil momentum which increase as L increases. This translates into the angular correlation and energy sharing distributions for the emitted nucleons to peak above and below the quasifree angle and energy.

A common practice in calculations involving two nucleon absorption or two nucleon transfer reactions is to assume that the nucleon pair have zero separation and are thus in a relative s state. It should be noted that such factorized calculations using harmonic oscillator wave functions to describe the center-of-mass motion of the pair have effectively decoupled the relative and center-of-mass motion quantum numbers. This can prove to be a powerful tool to extract the quantum numbers involved in the absorption process. The advantage of using a zero-range approximation is that it reduces the six dimensional integral in such calculations, to a three dimensional integral involving only the center-of-mass coordinates of the pair with respect to the spectator core. Hence, the zero-range approximation greatly simplifies theoretical calculations. The isospin of the transferred pair is assumed to be $T=0$ as in the real deuteron case. Antisymmetry between exchange of the two nucleons then requires the pn pair to be in a spin triplet ^3S state. The relative $l=0$ state of the pair also limits the possible values of the orbital angular momentum transfer, L, for the various nucleon shell couplings via parity considerations. By resolving the residual states in the recoil ^{14}N nucleus and using the known nuclear structure information of the target ^{16}O nucleus and recoil nucleus, information can be gained about the quantum numbers involved in the absorption process. In the impulse approximation the quantum numbers of the discrete states populated in the spectator ^{14}N nucleus are identically those of the pn pair at the time the photon is absorbed, since the target nucleus has spin $J=0$. The zero-range approximation then limits the absorption on two p-shell nucleons to be $L=0,2,4,\ldots$ due to parity considerations. However, it is possible to have absorption on a pn pair in a relative p wave or higher partial waves.

Significant nuclear structure information has been gained from two nucleon transfer reactions. Such measurements inspired Cohen and Kurath [9] to calculate the coefficient-of-fractional-percentage for two nucleon transfer in $1p$-shell nuclei. Their calculations predict that the $T=0$, 1^+ ground state of ^{14}N is predominantly $L=2$ orbital angular momentum transfer in character, while the $T=0$, 2^+, 7.03 and $T=0$, 3^+, 11.05 MeV states are purely $L=2$ orbital angular momentum transfer in character. The $T=0$, 1^+, 3.95 MeV state is predicted to be predominantly $L=0$ in character and the $T=1$, 0^+, 2.31 MeV state can only to be reached by $L=0$ transfer [10]. Although there is strong experimental evidence confirming the Cohen and Kurath predictions of the transferred angular momentum character to these states [10–12], some discrepancies do exist. Hoot *et al.* [13] determine from their DWBA analysis that in addition to the $L=0$ contribution they need the $L=2$ contribution to be twice the $L=0$ value as predicted by Cohen and Kurath in order to fit the 3.95 MeV state in ^{14}N. Data from a pion absorption experiment performed by Schumacher *et al.* [14], for an incident pion energy of $T_\pi = 116$ MeV, when compared to

their DWIA QD model calculation, find that a large $L=0$ contribution to the ground state is necessary to explain their energy sharing and angular correlation data. The number of L values required to describe an individual state need not be greater than two, at least in the case of the zero range approximation, as the contribution to the cross section decreases rapidly as the angular momentum quantum number increases. The dependence on the magnitude of the cross section with respect to the L transfer is nicely demonstrated by the $(p,p\alpha)$ transfer experiment of Jain *et al.* [15] using ^{6}Li and ^{7}Li target nuclei. They find the maximum in the cross section for the $L=0$ reaction on ^{6}Li is 5 times larger than the cross section for the $L=1$ reaction on ^{7}Li. In the pion absorption experiment of Schumacher *et al.*, they find a factor of 10 difference in the maximum of the angular correlation cross sections between the $L=0$, 3.95 MeV state and the predominant $L=2$ ground state as well as the pure $L=2$, 7.05 and 11.03 MeV states. Using such information, and the fact that we have limited solid angle coverage and limited available beam time, along with the desire to search for the elusive $T=1$, 2.31 MeV state, dictated that the current experiment be performed at the quasifree opening angle of the pn pair.

The electromagnetic interaction is an ideal probe of nuclear structure and is useful for exploring nuclear properties above the dominating mean field correlations. In particular it was originally hypothesized that real photons would be ideally suited to the study of short range correlations [4] due to the intrinsic large momentum mismatch for intermediate photon energies. It was predicted [16] that short range correlations can greatly influence the scale of the cross section by more than an order of magnitude, depending on the choice of the central correlation function. However the many assumptions which were made need to be further studied before any conclusive evidence of SRC's can be extracted by the comparison of this theory with measurements. In any case, to uncover clear evidence of nucleon-nucleon correlations above that predicted by the mean field will require a very good theoretical understanding of all possible processes contributing to the two-nucleon absorption mechanism.

Recently the effect of nucleon-nucleon correlations upon electromagnetically induced proton-neutron knockout has been theoretically revisited [17]. The authors investigate the effect of the state independent Jastrow correlations resulting from the hard core part of the nucleon-nucleon potential and the state dependent correlations due to the tensor part of the nucleon-nucleon potential. To investigate these effects, they calculate cross sections for the exclusive $^{16}\mathrm{O}(e,e'pn)^{14}\mathrm{N}$ reaction in superparallel kinematics. The advantage of superparallel kinematics is that the W_{TT} and W_{LT} structure functions do not contribute to the cross section, making interpretation of the results more clear. Furthermore, the choice of kinematics resulted in $\epsilon=0.951$, which characterizes the longitudinal component of the photon, while the value of the four momentum transfer squared was $Q^2=0.0536$ GeV$^2/c^2$. Using these kinematics, with the assumption of dipole scaling of the form factors, results in the W_L structure function contributing $\sim$90% to the cross section while the transverse structure function only contributes $\sim$10%. The results of their calculations are quite striking. The state independent short range correlations contribute only modestly to the enhancement of the cross section to discrete states in the residual ^{14}N nucleus. However, the state dependent tensor correlations (corresponding to a pn pair in a $^3S_1$ configuration) are seen to result in a factor of 2 increase to the 1^+, 3.95 MeV and ground states where such a $^3S_1$ pair configuration is possible. The effect of tensor correlations to the 0^+, $T=1$, 2.31 MeV state, where a $^3S_1$ pair configuration is not possible, and the 2^+, 7.03 MeV state is seen to only marginally contribute to an increase in the cross section.

Previous studies [18,19] by the same authors also investigated the effects of nucleon-nucleon correlations for the case of real transverse photons. Their microscopic calculation uses continuum and bound state wave functions generated in the same mean field potential. This maintains orthogonality between initial and final state wave functions and excludes spurious contributions entering into their calculations. They use the two body overlap amplitudes for p-shell nuclei of Cohen and Kurath [9] to describe the two-hole character of the ^{14}N nucleus with respect to the ^{16}O ground state. Both spin independent and spin dependent correlation functions are then included to describe correlations in the ^{16}O nucleus. Apart from taking distortions of the ejected nucleons into account, this microscopic calculation can evaluate the contribution of competing processes such as meson-exchange and Δ-isobar currents separately. It is also worth noting that in such a formalism no separation between relative and center-of-mass motion can be made as this can only be achieved in a harmonic oscillator basis. The predictions of these calculations will be compared to the present experimental results.

II. EXPERIMENTAL PROCEDURE AND DATA ANALYSIS

The measurement described in this paper was carried out using the tagged photon spectrometer facility [20] at the Saskatchewan Accelerator Laboratory (SAL). A 206 MeV electron beam was extracted from the pulse stretcher ring [21] with duty factors of approximately 80%. The electrons were directed onto a 115 μm thick Al radiator. Electrons which had undergone a bremsstrahlung process were momentum analyzed by the spectrometer magnet and were detected on the 62-channel tagger focal plane. The tagged photon energy range was primarily $E_\gamma=98.5$ to 141.0 MeV. Some additional running was at photon energies of $E_\gamma=61.0$ to 117.0 MeV in order to measure the neutron detection efficiency over a larger range of neutron energies. The relatively high duty factor enabled tagging rates of $(1-2)\times10^8$ photons/sec. The tagging efficiency, defined as the ratio of the number of photons incident on the target to the number of electrons detected in the tagger focal plane, was measured by reducing the electron beam intensity by 3 orders of magnitude and then counting the number of photons incident on a lead glass detector which had a 100% detection efficiency. Tagging efficiencies, normally measured every 12 hours, were typically about 53% for the photon energy range $E_\gamma=98.5$ to 141.0 MeV.

After exiting the tagging magnet, the photon beam was

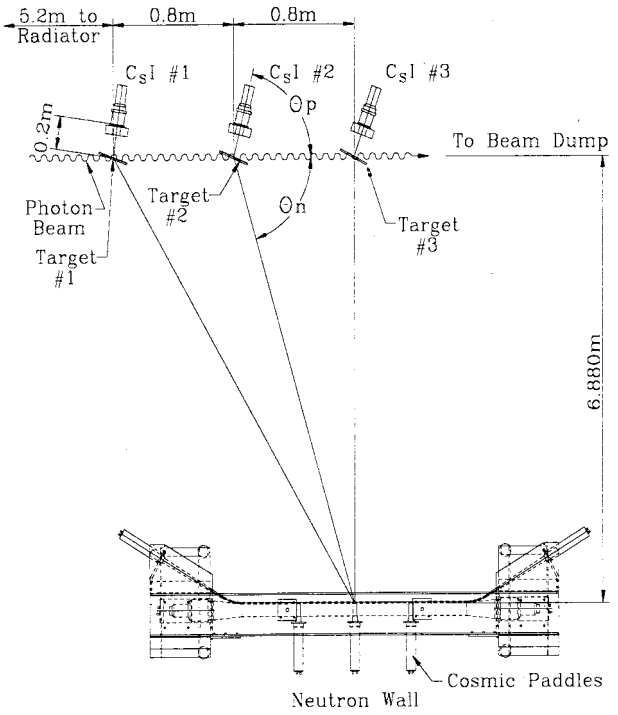

$\Theta_{opening} = 160^{\circ}$ ($E_{\gamma} = 120$MeV)

	CsI #1	CsI #2	CsI #3
Θp	82°	76°	70°
Θn	77°	83°	90°

FIG. 1. General overview of the experimental setup (not to scale).

collimated and then passed through three identical target samples before entering a well shielded beam dump. The targets were constructed from 1 mm thick Al frames hollowed in the form of an ellipse. Thin 7.6 μm Kapton windows were used to contain the heavy water (93% D_2O, 7% DO) and distilled water targets. Three empty targets of identical design were also constructed so that measurements with these targets could be subtracted from the full target samples to remove the background resulting from the target windows and the air surrounding the targets. To minimize energy loss of the protons in the targets, the targets were set at angles from 24 to 32° relative to the beam direction. This resulted in elliptical photon illumination profiles with axes approximately 10 cm by 4 cm on each target sample.

The experimental geometry is depicted in Fig. 1. The opening angle was chosen to match the opening angle for deuterium kinematics near the center of the photon energy range studied. This was also expected to be a good approximation of the quasifree opening angle expected for the emission of correlated proton-neutron pairs from ^{16}O. Protons were detected in high resolution Δ-EE telescopes. The Δ-E detectors consisted of 2.0 mm thick NE102A plastic scintillators. The PMT signals from these detectors were input to a CFD, the output of which was used as a common start for both the tagging focal plane detector TDC's and for the neutron detector TDC's. The E detectors were CsI(Tl) scintilla-

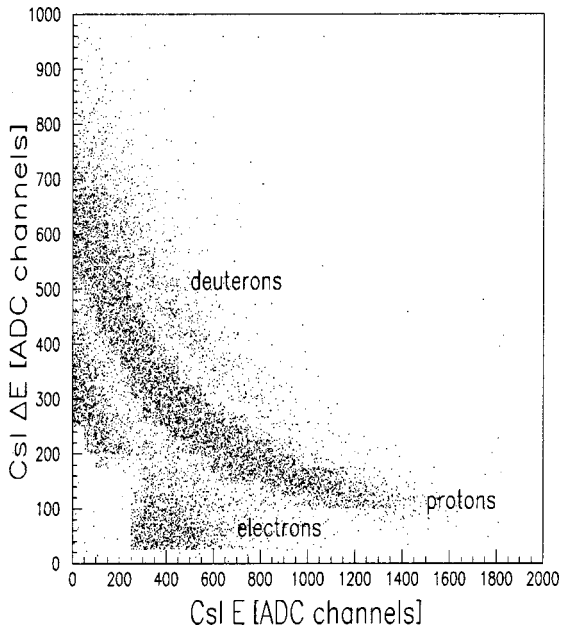

FIG. 2. A typical scatter plot for one of the proton telescopes. The energy deposited in the Δ-E detector is plotted as a function of the energy deposited in the CsI E detector. Clear particle bands are depicted. Also shown in the bottom left-hand corner of the figure is the effect of the hardware box cut.

tion crystals 7.61 cm in diameter and 7.61 cm in length and were capable of stopping ~165 MeV protons incident normal to the front face of the detector. The threshold for proton detection was ~21 MeV. The proton polar angular acceptance was $\Delta\theta_p = \pm 7.5^{\circ}$ for a point target. However, the elliptical beam spot on the target and the assumed Gaussian distribution for the photon beam profile resulted in a Gaussian distribution of proton angles such that 95% occurred within $\Delta\theta_p = \pm 15^{\circ}$. The azimuthal angular acceptance was also a Gaussian distribution such that 95% occurred within $\Delta\phi_p = \pm 10^{\circ}$. The proton solid angles, corrected for the finite size of the beam spot on the target, were approximately 57 msr.

Protons were identified by comparing the partial energy deposited in the Δ-E detector and the remainder of the particle's energy deposited in the CsI(Tl) detector. This resulted in characteristic particle bands in the scatter plot shown in Fig. 2. Good separation of protons from deuterons and electrons is demonstrated. In the lower left hand corner of Fig. 2 the effect of a hardware box cut is evident. This cut served to prevent the numerous events triggered by low energy electrons from being written to tape through the use of a fast clear. The long decay time of the CsI(Tl) scintillator pulse ~1 μs limited the maximum tagging rate due to pileup in these detectors. The level of pileup was kept below 3% during the experiment and the data were corrected for this effect. Due to the poor resolution of CsI(Tl) detector number three, only data taken from detectors one and two were included in the data analysis.

The neutron energy was measured by a time-of-flight (TOF) method where the typical flight distances were ~7 m. The neutron detector consisted of an array of ten

BC400 plastic scintillator bars, with dimensions 1.5 m $\times 0.15$ m$\times 76$ mm (thick), which were viewed at each end by photomultiplier tubes. Situated directly in front of the neutron array were veto detectors with dimensions 1.5 m $\times 0.15$ m$\times 3$ mm (thick) which were also viewed at each end by PMT's. Candidate neutron events were identified by a signal from a neutron bar with no signal in the corresponding veto detector. The neutron detector covered an angular range of $\sim \pm 6°$ in θ and ϕ, and due to its large distance from the target saw virtually a point target. The geometrical solid angles for the neutron detector subtended by targets number one and two were 45.3 and 47.1 msr, respectively. The position of particles detected along the length of each bar was determined from time division. A coincidence with discrete cosmic ray detectors placed above and below the neutron array enabled calibration of this positional information. The resulting uncertainty in the angular resolution inferred from this measurement was $\Delta\theta_n < 1.0°$.

The cosmic ray events also enabled the calibration of the energy deposited in the neutron bars in units of electron-equivalent energy (MeV_{ee}). In the analysis of real and simulated neutron events the energy deposited by recoil protons was expressed in MeV_{ee} by assuming that the light output response of NE102 was the same as that for BC400. This was necessary due to the lack of existing data for the light output of BC400. The similarity in the two scintillator materials makes this approximation reasonable. The formula used to convert the nonlinear proton energy loss into the corresponding electron-equivalent energy was [22]

$$E_{ee} = 0.95T_p - 8.0[1 - \exp(-0.10T_p^{0.90})], \qquad (1)$$

where T_p is the proton kinetic energy, and E_{ee} is the deposited energy in MeV_{ee}. A 2 MeV_{ee} threshold of the deposited energy was applied to all neutron bar events and was a factor in the determination of the neutron detection efficiency.

Using the deuterium present in the heavy water, it was possible to measure the neutron detection efficiency simultaneously with the primary $^{16}\mathrm{O}(\gamma,pn)^{14}\mathrm{N}_{0,1,2,\ldots}$ measurement. Simulations were necessary to remove acceptance effects due to the photon energy dependence of the deuterium kinematics as well as the geometrical acceptance effects of the extended target. The extended target tended to wash out to a large degree the acceptance effects due to deuterium kinematics. These effects are demonstrated in Table I for the combination of CsI number one and the neutron array. The column F_{Acc}^{pt} in Table I represents the ratio of events in the neutron detector to the corresponding number of events in the proton detector for deuterium kinematics, assuming 100% detection efficiency for both detectors and a point target. From this column it is evident that the opening angle favors a photon energy of about 130 MeV. The column F_{Acc}^{ext} represents the same ratio but with the extended target now included in the simulation. The gradual lowering of the ratio of acceptances for deuterium kinematics has been virtually removed by the effects of the extended target. To extract the neutron detection efficiency independent of the experimental geometry the measured efficiencies were divided by the factor F_{Acc}^{ext}. The detection efficiency results of the neutron array for one of the CsI detectors is shown in Fig. 3.

TABLE I. Parameters necessary to unfold the neutron detection efficiency from the experimental measured efficiency for CsI detector number 1 ($\theta_p = 82°$). The errors given represent the statistical error of the measurement only.

E_γ^{Sim} (MeV)	E_γ^{Tag} (MeV)	F_{Acc}^{pt} (%)	F_{Acc}^{ext} (%)	Exp. eff. (%)	T_n^{Tag} (MeV)	Net eff. (%)
65	67	0.45	0.34	6.0±0.3	32.7	17.6±0.9
75	82.5	0.51	0.37	5.8±0.4	40.1	15.7±1.1
85	97.4	0.58	0.37	5.4±0.4	47.9	14.6±1.4
105	103.7	0.70	0.38	4.5±0.2	51.7	11.8±0.5
115	115.6	0.73	0.38	4.8±0.2	57.7	12.6±0.5
125	126.7	0.75	0.38	4.4±0.3	63.2	11.6±0.8
135	137.4	0.75	0.38	4.4±0.3	68.5	11.6±0.8

The neutron efficiencies measured in this experiment can be compared with the results of Ref. [23] for NE102 scintillator with a 2 LU threshold applied to the later data set. The unit of 1 LU is defined to correspond to the half height of the 1.28 MeV γ-rays Compton edge obtain from a ^{22}Na source. This translates into approximately a 2.6 MeV_{ee} threshold for the NE102 measurement. The two data sets agree within the statistical errors for all neutron energies except the lowest neutron energy bin, where the current measurement predicts about a 15–20 % larger efficiency than for the NE102 measurement. Other authors [24] find that the half height choice in the Compton edge calibration point leads to an energy calibration point which is larger than the Compton edge en-

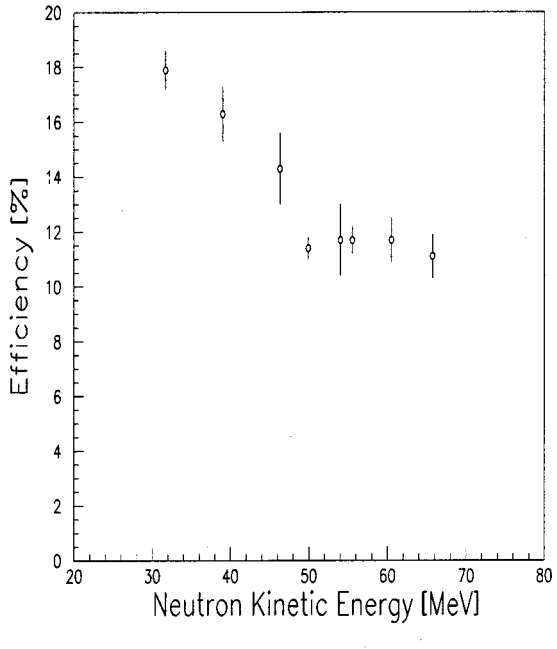

FIG. 3. The unfolded or net neutron detection efficiency versus the neutron kinetic energy for CsI number 2, $\theta_p = 76°$. A 2 MeV_{ee} threshold of the deposited energy has been applied. The error bars are statistical only.

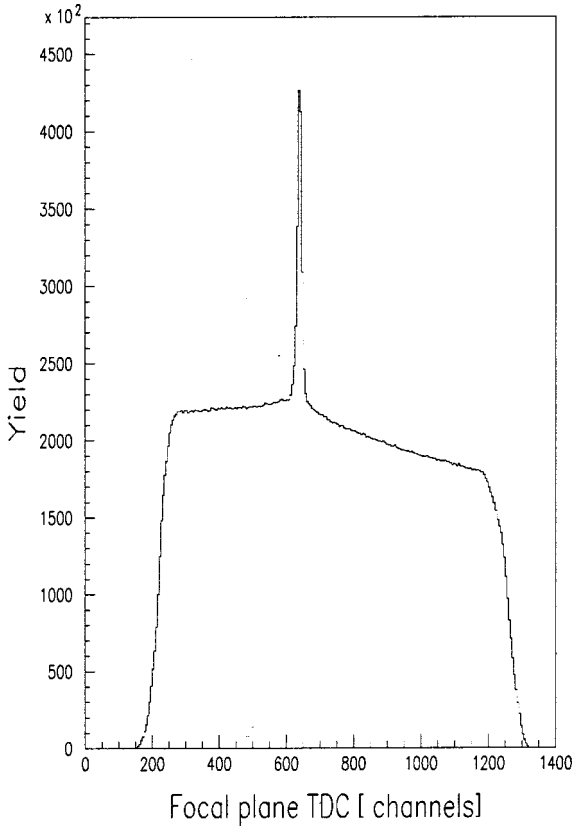

FIG. 4. The tagger TDC spectra with all 62 channels aligned for one of the CsI telescopes. The timing resolution is approximately 1.6 ns FWHM.

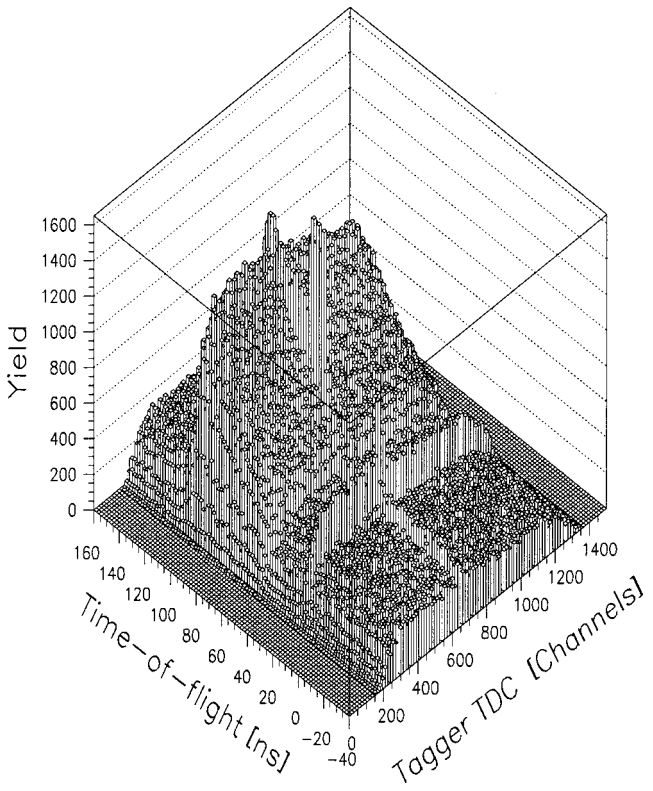

FIG. 5. Neutron time of flight versus the tagger TDC showing the regions of prompt and random coincidences.

ergy. They find that the 2/3 height represents a better choice for the Compton energy. This would then imply that the NE102 threshold of 2.6 MeV_{ee} is actually larger and may explain some of the discrepancies at the lower neutron energy. The weighted average neutron efficiencies for the 3.95 MeV state were 14.4% and 14.3% for CsI detectors number one and two, respectively. The estimated systematic uncertainty in the neutron detection efficiency is 7%.

The particle's energy determined by the neutron array was calibrated independently from the photon tagger by locating the gamma flash in the neutron TDC spectrum and using the known target to neutron detector distance. By using the overdetermined kinematics from the two body breakup of the deuterium, the tagged photon energy corresponding to each of the 62-channel focal plane detectors could be calibrated. The photon energy resolution was typically $\pm$ 0.5 MeV. The FWHM timing resolution of the gamma flash was 0.9 ns.

In this experiment the signal from one of the proton Δ-E detectors was used as a TDC start for the tagger focal plane electronics. The tagger electronics then determined if a coincident post-bremsstrahlung electron was detected within a fixed resolving time. During this time the photon tagger scalers were inhibited so that there was no dead time correction necessary for the photon flux normalization. A real proton-electron coincidence resulted in a prompt peak in the spectrum of the tagger TDC's as is evident in Fig. 4. All tagger channels are shown together, resulting in a FWHM timing resolution of 1.6 ns. The prompt peak rests on a random-coincidence background. In a simple one-arm experiment the contribution from these random coincidences may be removed by generating a spectrum (such as an excitation energy spectrum) of events in a TDC time window that includes the prompt peak, and a spectrum for a time window that does not include the prompt peak. Subtraction of the properly-normalized random spectrum from the prompt-random spectrum results in the spectrum for true electron proton coincidences.

For a triple coincidence experiment a much more complicated situation arises. Depicted in Fig. 5 is a plot of the neutron array TOF versus the tagger TDC. This spectrum was accumulated under the condition that the energy deposited in the neutron detector be larger than 2 MeV_{ee}, which was seen to significantly reduce the level of random neutron events. The narrow ridge, at a neutron TOF of 23 ns, running parallel to the tagger TDC axis corresponds to the gamma flash used to calibrate the neutron array and is not a source of background to the prompt triple coincidences.

Unlike the simple picture which exists for double coincidence experiments there are five combinations of correlated and uncorrelated signals for the case of a triple coincidence. They are as follows. (1) The true coincidence peak where all three particles are correlated, appears as a ridge running parallel to the neutron TOF axis. This ridge starts at a neutron TOF of 55 ns and continues to TOF values of 200 ns which is the dynamic range of the TDC. (2) Events in which the proton and electron are correlated but the neutron is not correlated, appear as a ridge running parallel to the neutron TOF

axis and covers the entire range of neutron TOF values. The level of this background is constant throughout the entire TOF spectrum. Events making up this ridge which occur before the gamma flash require velocities greater than the speed of light and therefore must be purely random. Analysis of this region determined the correct level of this component of the background to be subtracted from the prompt region. (3) Events in which the neutron and proton are correlated but the electron is not correlated, appear as a dominant ridge running parallel to the tagger TDC axis. Due to the high tagging rates in this experiment this is the major source of random coincidence background to the prompt region. (4) Events in which the electron and neutron are correlated and the proton is not would be a seen as a ridge running at a 45° angle to the random electron and random neutron ridges. This is possibly obscured by the dominant ridge of background events in which the electron was random. (5) Finally the entire spectrum rests on a uniform background of events in which all three particles are uncorrelated.

The distribution of the random background events was determined as a function of neutron TOF values in the following manner. A tagger TDC spectrum was made for each 10 ns bin of neutron TOF values. The bin size was chosen for statistical reasons. For kinematically allowed neutron TOF's the level of the random background beneath the prompt peak was determined. To these values a constant level of background neutron events was added by determining the prompt yield of neutrons occurring in the time region before the gamma flash. This procedure produced a random tagger TDC spectrum as a function of neutron TOF which included all classes of random events. An advantage to this method is that it effectively accounts for the neutron detection efficiency to both the prompt-random and random excitation energy spectra, so that once a subtraction is made only the correct yield of prompt events is left. For large TOF values or low neutron energies the neutron detection efficiency varies rapidly. However the 10 ns bin corresponds to only a 2–3 MeV range in neutron energy and so the detection efficiency can be assume to be constant to a good approximation for this small energy bin. For large neutron energies (or correspondingly small TOF's) the 10 ns bin corresponds to a 7–8 MeV bin in neutron energy. Here however, the neutron efficiency is seen to be constant for neutron energies greater than ~50 MeV (see Fig. 3).

The excitation energy of the recoil nucleus is given by

$$E_x = E_\gamma - T_p - T_n - T_r - Q, \tag{2}$$

where E_x is the excitation energy of the A-2 recoil nucleus, Q is the reaction threshold (=22.96 MeV), E_γ is the photon energy, and T_p, T_n and T_r are the proton, neutron and recoil nucleus kinetic energies, respectively. The random background contribution to the excitation energy spectra was generated as follows. For each prompt event 100 random background events were generated by choosing a random proton energy and a random neutron TOF. The proton energy was chosen by sampling the measured proton energy distribution for events outside the prompt tagger TDC region. The random neutron TOF was found by sampling the distribution which was determined as outlined in the previous paragraph. The 10 ns neutron TOF bin was too large to reproduce, in the randomly generated neutron TOF spectrum, the sharp rise and fall seen in the prompt neutron TOF spectrum. It was therefore necessary to impose a cut on the neutron kinetic energies so as to avoid these areas. This resulted in a kinematical acceptance of neutron energies 25 MeV$\leqslant T_n \leqslant$80 MeV. Considering the photon energies involved, this kinematical cut did not appreciably influence the phase space acceptance of coincident proton-neutron events, resulting from the $^{16}\mathrm{O}(\gamma,pn)$ reaction, in which the neutron was ejected without undergoing a final state interaction (FSI). By isotropically choosing a random hit position for the neutron in the neutron array, the random neutron momentum could be generated. Using this information and the proton momentum, the recoil energy, T_r, could then be determined for the random spectrum. For the prompt-random spectrum the actual measured nucleon momenta were used to calculate T_r. An excitation energy spectrum for the empty target was made in a similar fashion and after being suitably scaled was subtracted from the foreground spectrum. The empty target contribution was typically no greater than a few percent of the foreground for any given bin.

For the exclusive $^{16}\mathrm{O}(\gamma,pn)^{14}\mathrm{N}_{0,1,2,\ldots}$ reaction the cross sections were computed by the following equation:

$$\frac{d\sigma}{d\Omega_p d\Omega_n} = \frac{Y_{pn} A \sin(\theta) N_R}{N_e d\Omega_p d\Omega_n \varepsilon_{eff} \varepsilon_{tag} (\rho t) W_0 N_0 \varepsilon}, \tag{3}$$

where Y_{pn} is the yield of coincident proton-neutron pairs, A is the atomic mass of the target, θ is the target rotation angle with respect to the incident photon beam, N_e is the yield of electrons detected in the tagger focal plane, $d\Omega_p$ and $d\Omega_n$ are the geometrical solid angles (corrected for the finite size of the beam spot on the target) subtended by the proton detector and the neutron detector, respectively, ε_{tag} is the tagging efficiency, $N_0 \rho t$ is the number of target nuclei per cm^2 (the target thickness was assumed to be the desired 1 mm thick), N_0 is Avogadro's number and ε accounts for the correction necessary for pile-up and proton misidentification due to nuclear interactions in the CsI detector, ε_{eff} is the measured neutron detection efficiency and W_0 is the corresponding weight of oxygen atoms in the heavy water. The measured deuterium cross sections were compared to the Rossi *et al.* parametrization [25] of the existing experimental data in order to determine the absolute target thickness. That is, the target thickness normalization constant, N_R, is defined via the relation $(d\sigma/d\Omega_p)_{Rossi} = N_R (d\sigma/d\Omega)_D$. The uncertainty in the number of target nuclei is estimated to be 7%. The net systematic error in the measurement is 11%.

Many cross sections reported for two nucleon emission experiments simply use the product of the geometrical solid angles $d\Omega_p$ and $d\Omega_n$. However, this is only valid for completely uncorrelated particles and can lead to confusion when comparing experimental results with less than 4π solid angle coverage. In order to compare cross sections determined in such a manner with theory, the use of the geometrical solid angles must be accounted for by using the theoretical predictions in a Monte Carlo simulation which includes the exact

detector geometry and thresholds. For comparison with previous results the present cross sections will also be quoted differential in both the proton and neutron solid angles where the geometrical values are used.

However, if the angular correlation between the pn pair is known for a given state, it is possible to determine the cross section differential in only the proton solid angle. The correlation function can be used to effectively integrate over the neutron solid angle. That is, an event in the proton detector, folded in with the angular correlation, dictates all the possible phase space which is available to the neutron. The angular correlation function for the 3.95 MeV state has been experimentally measured to be Gaussian in shape [14,26,27] reflecting the almost pure $L=0$ character of this state. The width of the angular correlation for an $L=0$ state can be estimated to be $\tan^{-1}(k_f/k_n)$, where k_f is the Fermi momentum of the two nucleon system and k_n is the average momentum of the ejected nucleons. With the average nucleon kinetic energy for the 3.95 MeV state in ^{14}N being 45 MeV and using k_f to be the single nucleon Fermi momentum divided by the square root of two, the width of the angular correlation distribution for this state should be approximately 30°. The assumption that the detectors are set exactly at the quasifree angle would contribute at most $\pm 7\%$ error in the determination of the cross section for a point target with reasonable shifts of the detectors away from the quasifree angle. Note, however, that in the same way that the extended target smears the angular correlation for deuterium kinematics as a function of the photon energy, the cross section determination is virtually insensitive to reasonable shifts of the detectors away from the quasifree angle.

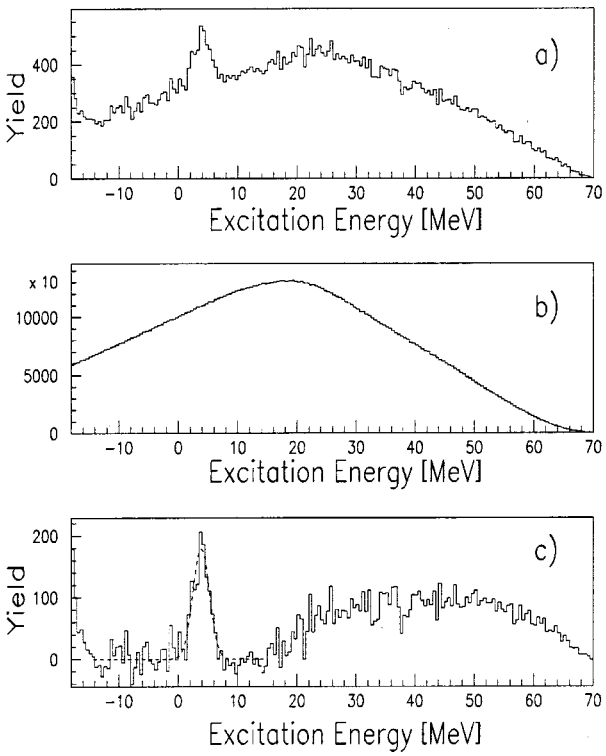

FIG. 6. The excitation energy spectrum for the ^{16}O$(\gamma,pn)^{14}$N reaction. The data were accumulated for the photon energy range from 98.5 to 141.0 MeV. Figure (a) was constructed with a cut on the photon tagger TDC prompt peak. Figure (b) represents the random background contribution. Figure (c) is the net missing energy yield spectrum with the random contribution subtracted.

III. RESULTS AND DISCUSSION

The resulting excitation energy spectrum for the ^{14}N nucleus is shown in Fig. 6(c) for both CsI detectors combined. Figure 6(a) shows the foreground together with the random background while Fig. 6(b) depicts the shape of the random background contribution generated as discussed in the preceding section. In the far left of Figs. 6(a) and 6(c) the right hand shoulder of the ^{2}H peak is evident. For clarity only the shoulder of this dominant ^{2}H peak is shown. By noting the difference in reaction Q values between the ^{2}H(γ,pn) and ^{16}O$(\gamma,pn)^{14}$N$_0$ reactions, the peak observed at low excitation energy can be unambiguously identified as the $T=0$, 1^+, 3.95 MeV state. The FWHM energy resolution of this state is 2.8 MeV. The clean separation between the low excitation energy region assumed to have a $(1p)^{-2}$ shell model configuration and the start of the continuum considered to be a $(1p)^{-1}(1s)^{-1}$ shell coupling is seen as experimental evidence that the minimal shell removal energy is 20 ± 2 MeV for a $(1p)^{-1}(1s)^{-1}$ pair coupling. This is in good agreement with values inferred from quasielastic $(e,e'p)$ scattering data.

From Fig. 7, which depicts only the low excitation energy region of Fig. 6, it is clear that only the $T=0$, 1^+, 3.95 MeV state is strongly excited. On the contrary the $T=0$, 1^+ ground state is not significantly populated. According to the predictions of Cohen and Kurath the difference between the two states lies in the preferred angular momentum transfer. The ground state is reached by a predominantly $L=2$ transfer while the 3.95 MeV state is predominantly $L=0$ in nature. Given that this experiment was performed near quasifree kinematics and that the peak in the cross section for $L=2$ transfer is greatly reduced from the $L=0$ transfer cross section, the results are consistent with the Cohen and Kurath predictions. The 2^+, 7.03 and the 3^+, 11.05 MeV states, both $T=0$, are predicted to be reached by pure $L=2$ transfer and are also not evident in the spectrum.

The results of Schumacher *et al.* [14] indicated sensitivity to $L=2$ absorption at the quasifree angle which was comparable to $L=0$ absorption at an angle 20° larger than the quasifree angle. Using their extracted form factor data for the various states and the above observation, it can be inferred that the ^{16}O$(\gamma,pn)^{14}$N$_{0,2,3}$ measurement of Isaksson *et al.* [28], where the three states observed were comparable in magnitude, had a recoil momentum acceptance of $P_R=\sim 150$ MeV/c. Here $L=0$ absorption is down by an order of magnitude as compared with the peak in the angular correlation cross section. The results of the present measurement are consistent with a recoil momentum acceptance $P_R=\sim 90$ MeV/c which is statistically a reasonable place to search for $T=1$ absorption. However, the $T=1$, 0^+, state at 2.31 MeV is not seen to be significantly populated as this would be indicated by a shoulder to the left of the 3.95 MeV state. As the 2.31 MeV state is reached by a pure $L=0$ trans-

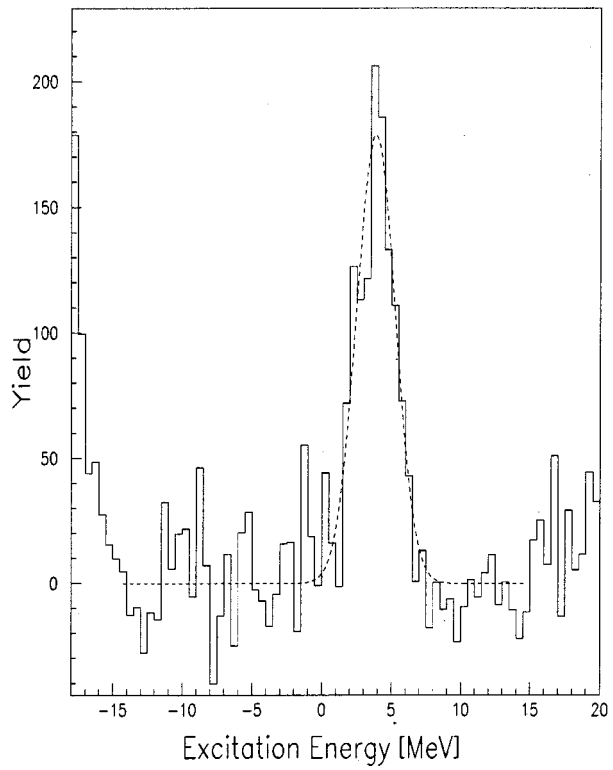

FIG. 7. The yield spectrum for both CsI detectors for the excitation range from −18.0 MeV to 20 MeV. The discrete state at 3.9 MeV is identified with the 3.95 MeV $(1^+,0)$ level in ^{14}N. Significant yield in the continuum begins at approximately 20 MeV and is thought to consist of removal of a *p*-shell and of a *s*-shell coupled nucleon pair in the (γ,pn) reaction. The results seem to indicate a clean measurement of the minimal shell removal energy for a coupled *p* and *s* shell nucleon pair. Accounting for the excitation energy resolution, the minimal shell removal energy is estimated to be 20 ± 2 MeV.

fer, which favors the detection phase space acceptance of this experiment, absorption on a $T=1$ nucleon pair is estimated to be less than 10% of the cross section to the 3.95 MeV state. Although absorption on $L=2$ pairs is not evident in the present measurement, absorption on $L=2$ pairs has been previously demonstrated [28].

As a consequence of the absence of the $L=2$ angular momentum transfer states, it is assumed that the contribution to the cross section by absorption on nucleon pairs with center-of-mass motion characterized by $L=2$ $(L>2)$ is small (negligible) for the angular region of approximately $\pm15°$ around the quasifree angle. Applying the zero-range approximation, $l=0$, parity and antisymmetry relations to the present results, and noting $T=1$ absorption is suppressed, restricts the quantum numbers so that a $(1p)^{-2}$ nucleon pair must be uniquely determined as $L=0$, $S=1$, and $T=0$. This approximation when applied to the continuum implies that the quantum numbers for a $(1p)^{-1}(1s)^{-1}$ pair coupling are $L=1$, $S=1$, and $T=0$ while those for a s^{-2} pair are the same as those for a $(1p)^{-2}$ pair. However, in a recent measurement of the ^{12}C(γ,pn) reaction [29] for the photon energy range $E_\gamma=120-150$ MeV the angular distribution of the detected pn pairs was observed to be different from the deuterium case. The authors interpret this as evidence for the fact that the quasideuteron assumption does not fully describe the photoabsorption on proton-neutron pairs in nuclei. The zero-range assumption therefore may not be reasonable in light of this recent result. Relaxing the zero-range approximation and assuming absorption on nucleon pairs $L\geqslant2$ is insignificant, for the present measurement, leads to the possibility that the nucleon pair can have a relative partial wave composition of $l=0,1,2$ for all possible nucleon shell couplings. If the restriction that $T=0$ is enforced, then the appropriate choice of the spin $(s=0,1)$ and center-of-mass motion $(L=0,1)$ of the pair, must be used for parity and antisymmetrization considerations for the specific relative partial wave composition. However, since no unnatural parity angular momentum transfer states have been measured the possibility for $L=1$ on $(1p)^{-2}$ or $(1s)^{-2}$ couplings or $L=0$ for $(1p)^{-1}(1s)^{-1}$ coupling seems unlikely. This then restricts the quantum numbers of the pair to be $T=0$, $s=1$ and $l=0,2$ with $L=0$ for $(1p)^{-2}$ or $(1s)^{-2}$ couplings and $L=1$ for a $(1p)^{-1}(1s)^{-1}$ coupling.

The ability to compare calculations to data for correlated particles has been examined [30] and demonstrated to be a significant task. In particular, comparing calculations made with the recoil momentum $P_R=0$ MeV/c was demonstrated to be an insufficient matching of phase space between experiment and calculation. This should not be too surprising as the experimental yield is identically zero for $P_R=0$ MeV/c. In fact the most important scaling variable of the cross section is P_R. This is nicely demonstrated by the pion absorption measurement [14] which measured the angular correlation for the 3.95 MeV state in ^{14}N at the quasifree angle and 20° out of plane at the quasifree angle. The angular correlation function still possessed a reasonable Gaussian-like distribution and had the approximate magnitude expected for the recoil momentum acceptance even at this extreme out of plane angle. This confirms the dominance of the scaling variable P_R in the data.

The measured cross sections, differential in the geometric proton and neutron solid angles, are given in Table II along with the results of the calculations described in Refs. [18,19]. Both sets of calculations were performed in coplanar kinematics for $\theta_p=82°$ and $\theta_n=-77°$ and for a photon energy $E_\gamma=120$ MeV. Furthermore, both sets of calculations contain MECs and Δ-isobar currents, and only differ on which type(s) of correlations are included, central or state dependent correlations. The calculations were performed with and without the inclusion of tensor correlations and an integration over the recoil momentum P_R was performed. The column with the superscript $cal2$ includes MECs and Δ-isobar currents as well as both central and tensor correlations, and was performed for various excited states of the residual ^{14}N nucleus. The column with the superscript $cal1$ differed from $cal2$ by omitting only tensor correlations from the calculation. It is known that central correlations are predicted to have only a marginal effect on the magnitude of the (γ,pn) cross section [18]. The magnitude of the tensor correlations was regulated by means of the tensor correlation function $f_{t\tau}(r_{12})$ from the variational ^{16}O calculations by Pieper *et al.*

TABLE II. The cross sections for the $^{16}O(\gamma,pn)^{14}N_{0,1,2\ldots}$ reaction resulting from the current measurement are listed. The photon energy range was from 98.5 to 141.0 MeV. The data were taken near the expected quasifree opening angle of the nucleon pair. An upper estimate of the cross section for the ground state, 2.31, 7.03, and the 11.05 MeV states is given by asterisk (*) in the table and is used to signify that the cross section to these states is $<10\%$ of the value for the 3.95 MeV state. The yields listed for the energy range 0–20, 20–45, and 45–70 are meant to represent the approximate contributions to the cross section from 2 *p*-shell nucleons, 1 *p*-shell and 1 *s*-shell nucleons, and 2 *s*-shell nucleons, respectively. The errors stated with the measured cross sections are statistical in nature and are also meant to reflect the error in the peak fitting procedure and the error in the random background subtraction. The calculations labeled with superscripts $cal1$ and $cal2$ are the results of Refs. [18,19], without and with the inclusion of tensor correlations, respectively. The value in parenthesis has been averaged over the detector acceptances in order to compare with the measured cross section.

State (MeV)	$d^2\sigma/d\Omega_p d\Omega_n\|^{cal1}$ (μb/sr^2)	$d^2\sigma/d\Omega_p d\Omega_n\|^{cal2}$ (μb/sr^2)	$d^2\sigma/d\Omega_p d\Omega_n$ (μb/sr^2)	θ_p (deg)
0.00		0.32	*	82
2.31		1.05	*	82
3.95	7.25 (5.94)	6.92	8.82 ± 0.74	82
7.03		0.20	*	82
11.05			*	82
E_x (MeV)			Yield	θ_p (deg)
0–20			682	82
20–45			2329	82
45–70			1601	82
0.00			*	76
2.31			*	76
3.95	6.55		6.89 ± 0.64	76
7.03			*	76
11.05			*	76
E_x (MeV)			Yield	θ_p (deg)
0–20			563	76
20–45			2143	76
45–70			1648	76

[31]. The results of the calculation, $cal2$, for these point kinematics reflect well the magnitude of the observed and unobserved states measured. The $T=1$, 0^+, 2.31 MeV state which is predicted to be about 14% of the 3.95 MeV state is not evident in the data. However, the statistical accuracy of the current measurement can only exclude absorption on $T=1$ pairs to be less than 10% of the 3.95 MeV state. The predominant $L=2$ ground state and pure $L=2$, 7.03 MeV are predicted to be more than a factor of 20 suppressed compared to the $L=0$, 3.95 MeV state making the calculation and measurement consistent with the absence of these states.

TABLE III. Angular correlation results from calculations from Refs. [18,19] without (*cal*1) and with (*cal*2) the inclusion of tensor correlations. For comparison the plane and distorted wave calculations of the QD model described by Schumacher *et al.* [14] are also given. The proton angle was $\theta_p=82°$ and the photon energy was $E_\gamma=120$ MeV.

Calculation	$\theta_{opening}$ (deg)	FWHM (deg)	P_{Recoil} (MeV/c)
cal1	160.1	38.0	228
cal2	159.9	30.8	223
QD_{DWIA}	159.6	26.9	175
QD_{PW}	156.9	28.0	146

The calculation given in the column with the superscript $cal1$ in Table II, includes MEC's, Δ-isobar currents, and SRC's contributions to the cross section, but excluded tensor correlations. The calculation was performed for the same point kinematics as stated above. The peak of the cross section is comparable for the two calculations, however, the width of the angular correlation is somewhat broadened without the inclusion of tensor correlations. This will be further discussed in the following paragraph. In order to account for the phase space correctly a calculation was performed over a fine grid of proton and neutron θ acceptances. Including a grid in ϕ would have required an unreasonable amount of CPU time and for reasons stated above was deemed unnecessary. The results of this calculation were fed into a GEANT Monte Carlo simulation of the detectors and a correctly phase space averaged value of the calculation was obtained (given in parenthesis in the table) for comparison with the measured data. A grid was only calculated for the $L=0$, 3.95 MeV state for $\theta_p=82°$ since it is expected that the measurement at $\theta_p=76°$, being close in angle, would result in a similar size effect for the phase space averaged cross section. This averaging resulted in an approximately 18% decrease over the central point calculation. The decrease is expected, as the calculated differential cross section peaks close to $\theta_p=82°$. The 5.94 μb cross section is 67% of the measured 8.82 μb cross section.

As discussed earlier, if the shape and the width of the angular correlation function are known along with the quasifree angle of the pair, it is possible to extract the cross section differential in only the proton solid angle. This would make comparison of the cross section between different measurements less ambiguous due to phase space matching considerations. The angular correlation results from the calculations of Refs. [18,19] are given in Table III. These calculations were performed in coplanar kinematics, for $E_\gamma=120$ MeV, $\theta_p=82°$ and various neutron angles. Also given for comparison are the predictions of the QD calculation of Schumacher *et al.* [14] using a final energy prescription to describe the choice of the on-shell cross sections used in the calculation. The calculation was also performed in coplanar kinematics with $E_\gamma=120$ MeV, $\theta_p=82°$ and for various neutron angles. Although QD calculations are known to have inherent normalization problems, the results of the

TABLE IV. The cross section for the $^{16}O(\gamma,pn)$ reaction to the 3.95 MeV state in ^{14}N differential in the proton solid angle. The proton angle was $\theta_p = 82°$. The subscript indicates the FWHM of the angular correlation distribution assumed to extract the measured cross section as predicted by the calculations labeled $cal1$ and $cal2$, respectively. The calculations are the same as described in Table II and have been integrated over the neutron detector solid angle.

State (MeV)	$d\sigma/d\Omega_p\|^{cal1}$ (μb/sr)	$d\sigma/d\Omega_p\|_{38.0°}$ (μb/sr)	$d\sigma/d\Omega_p\|^{cal2}$ (μb/sr)	$d\sigma/d\Omega_p\|_{30.8°}$ (μb/sr)
3.95	3.4 (2.8)	4.1 ± 0.8	2.2 (1.8)	2.9 ± 0.6

calculation have demonstrated the ability to qualitatively reproduce the angular correlation and energy sharing distributions [14] as well as other qualitative features of the data. The calculation labeled QD_{PW} in Table III gives the results for the plane wave QD predictions. The plane wave angular correlation peaks at more forward angles than the free deuterium case as is expected from consideration of momentum conservation. The inclusion of FSI's in the calculation labeled QD_{DWIA} shifts the angular correlation peak close to that expected for free deuterium kinematics. Also the inclusion of FSI's in the QD model is seen to increase the recoil momentum distribution while the angular correlation width is not significantly altered. These qualitative features are consistent with what was reported by Schumacher *et al.* [14]. The results of the microscopic calculations [18,19] without the inclusion of tensor correlations, shows a significant, measurable broadening of the angular correlation width compared to the calculation with the inclusion of tensor correlations. As mentioned earlier, the magnitude of the peak in the double differential cross section for the two calculations only differed by a few percent; however, the change in the width of the angular correlation results in a significant change to the magnitude of the cross section.

In light of the above discussion the quasifree opening angle was chosen to be 160° in order to extract $d\sigma/d\Omega_p$ from the data. However, from Table I the column labeled $F^{ext}_{Acc}(E_\gamma)$ demonstrates the virtual insensitivity of the experimental apparatus to the exact peak of the angular correlation cross section. Therefore reasonable shifts of the quasifree angle of the pair will have little effect on the extracted cross section. Of course, the same is not true for the width of the angular correlation distribution. The calculations for $\theta_p = 82°$ were integrated over all neutron angles and are presented in Table IV. Note that the shape of the angular correlation was assumed to have the same form as the in-plane predictions and this assumption was used for the out of plane intergrations for the extraction of both the theoretical and measured cross sections. The value in parenthesis accounts for the varying cross section across the acceptance of the detectors and is the value which should be compared with the experimental result. The value used for this correction is only exact for the calculation in which tensor correlations have been omitted and is assumed to be a reasonable approximation for the calculation which includes tensor correlations. It is interesting to note that the inclusion of tensor correlations reduces the calculated cross section by 55%. Obviously, the current measurement cannot distinguish between the two results. Unlike the increase of the theoretical predictions for the predominant longitudinal $(e,e'pn)$ cross section [17], due to the many processes involved in the transverse absorption channel, such as meson-exchange and Delta-isobar currents, it is not surprising that destructive interference between these processes and the inclusion of tensor correlations results. To extract the cross section from the data for comparison with theory, the correct angular correlation width appropriate for the specific calculation was used in the Monte Carlo simulation. The experimental value to be compared with the appropriate calculation is given in Table IV in the column following the theoretical value. The dominant error in the extracted experimental and theoretical cross sections lies in the assumption that the angular correlation function is assumed symmetrical for the out of plane integration. To account for this approximation a 20% error is assigned to the extracted experimental cross sections. Not surprisingly, there is again quite reasonable agreement between the theoretical and experimental values.

IV. SUMMARY AND CONCLUSIONS

Interpretation of the data in a harmonic oscillator basis allowed for the extraction of which quantum numbers are important for the two nucleon absorption process. Only the $T=0$, 0^+, 3.95 MeV state was observed with significant yield. Using this information in conjunction with the observation of no unnatural parity states at low excitation energy restricts the $T=0$ pairs to have relative quantum numbers $l=0,2$ and an angular momentum transfer quantum number $L=0$ for $(1p)^{-2}$ or $(1s)^{-2}$ couplings, and $l=0,2$ with $L=1$ for a $(1p)^{-1}(1s)^{-1}$ coupling. These are the same relative partial waves as are found for the free deuteron. Absorption on $T=1$ pairs can be ruled out at approximately the 10% level, while absorption on pairs in $L=2$ motion can also be ruled out at the same statistical level near the quasifree angle. The magnitude of the measured cross sections was compared with microscopic calculations with and without the inclusion of tensor correlations. The peak in the two calculated double differential cross sections, with and without the inclusion of tensor correlations, was found to be in good agreement with the results of the current measurement. Only a measurement of the angular correlation width can distinguish between the importance of tensor correlations in the theoretical calculations. In general the calculations are consistent with the observed and unobserved states populated in the residual ^{14}N nucleus.

ACKNOWLEDGMENTS

We would like to thank P.G. Roos for performing the QD calculations and for his consultations which were helpful in the interpretation of the results presented.

[1] J. Levinger, Phys. Rev. **84**, 43 (1951).
[2] M. Barton and J. Smith, Phys. Rev. **95**, 573 (1954).
[3] M. Barton and J. Smith, Phys. Rev. **110**, 1143 (1958).
[4] K. Gottfried, Nucl. Phys. **5**, 557 (1958).
[5] J.C. McGeorge *et al.*, Phys. Rev. C **51**, 1967 (1995).
[6] I.J.D. MacGregor *et al.*, Nucl. Phys. **A533**, 269 (1991).
[7] L. Van Hoorebeke *et al.*, Phys. Rev. C **42**, R1179 (1990).
[8] R. Ent *et al.*, Phys. Rev. Lett. **62**, 24 (1989).
[9] S. Cohen and D. Kurath, Nucl. Phys. **A141**, 145 (1970).
[10] D.G. Fleming, J.C. Hardy, and J. Cerny, Nucl. Phys. **A162**, 225 (1971).
[11] N.F. Mangelson, B.G. Harvey, and N.K. Glendenning, Nucl. Phys. **A117**, 161 (1968).
[12] A. Van Der Woude and R.J. De Meuer, Nucl. Phys. **A258**, 199 (1976).
[13] C.G. Hoot, D.K. Olsen, R.E. Brown, J.R. Maxwell, and A. Scott, Nucl. Phys. **A203**, 339 (1973).
[14] R.A. Schumacher *et al.*, Phys. Rev. C **38**, 2205 (1988).
[15] M. Jain, P.G. Roos, H.G. Pugh, and H.D. Holmgren, Nucl. Phys. **A153**, 49 (1970).
[16] L. Boato and M.M. Giannini, J. Phys. G **15**, 1605 (1989).
[17] J. Ryckebusch, S. Janssen, W. Van Nespen, and D. Debruyne, Phys. Rev. C **61**, 021603(R) (2000).
[18] J. Ryckebusch, D. Debruyne, and W. Van Nespen, Phys. Rev. C **57**, 1319 (1998).
[19] J. Ryckebusch and W. Van Nespen, in Fourth Workshop on Electromagnetically Induced Two-Hadron Emission, edited by P. Grabmayr and A. Lallena, Granada, Spain, 1999, CD-ROM edition.
[20] J.M. Vogt, R.E. Pywell, D.M. Skopik, E.L. Hallin, J.C. Bergstrom, H.S. Caplan, K.I. Blomqvist, W. Del Bianco, and J.W. Jury, Nucl. Instrum. Methods Phys. Res. A **324**, 198 (1993).
[21] L.O. Dallin, in *Proceedings of the Particle Accelerator Conference*, edited by F. Bennett and J. Kopta (IEEE, Chicago, 1989), p. 22.
[22] R. Cecil, B. Anderson, and R. Madey, Nucl. Instrum. Methods **161**, 439 (1979).
[23] R.A.J. Riddle, G.H. Harrison, P.G. Ross, and M.J. Saltmarsh, Nucl. Instrum. Methods **121**, 445 (1974).
[24] H.H. Knoxx and T.G. Miller, Nucl. Instrum. Methods **101**, 519 (1972), and references therein.
[25] P. Rossi, E. De Sanctis, P. Levi Sandri, N. Bianchi, C. Guaraldo, V. Lucherini, V. Muccifora, E. Polli, A. Reolon, and G. Urciuoli, Phys. Rev. C **40**, 2412 (1989).
[26] W.R. Wharton *et al.*, Phys. Rev. C **31**, 526 (1985).
[27] E.D. Arthur *et al.*, Phys. Rev. C **11**, 332 (1975).
[28] L. Isaksson *et al.*, Phys. Rev. Lett. **83**, 3146 (1999).
[29] T.T-H. Yau *et al.*, Eur. Phys. J. A **1**, 241 (1998).
[30] D.G. Ireland, I.J.D. MacGregor, and J. Ryckebusch, Phys. Rev. C **59**, 3297 (1999).
[31] S. Pieper, R. Wiringa, and V. Pandharipande, Phys. Rev. C **46**, 1741 (1992).